

THE COSMIC SHEAR STIS PARALLEL PROGRAM - FIRST RESULTS

H. HÄMMERLE^{1,2}, J.-M. MIRALLES^{1,3}, P. SCHNEIDER^{1,2}, T. ERBEN^{2,4,5},
R.A.E. FOSBURY³, W. FREUDLING³, N. PIRZKAL³, S.D.M. WHITE²

¹*Institut für Astrophysik und Extraterrestrische Forschung der Universität Bonn, Auf dem Hügel 71, D-53121 Bonn, Germany*

²*Max-Planck-Institut für Astrophysik, Karl-Schwarzschild Str. 1, D-85748 Garching, Germany*

³*ST-ECF, Karl-Schwarzschild Str. 2, D-85748 Garching, Germany*

⁴*Institut d'Astrophysique de Paris, 98bis Boulevard Arago, F-75014 Paris, France*

⁵*Observatoire de Paris, DEMIRM 61, Avenue de l'Observatoire, F-75014 Paris, France*

Abstract. Since the Universe is inhomogeneous on scales well below the Hubble radius, light bundles from distant galaxies are deflected and distorted by the tidal gravitational field of the large-scale matter distribution as they propagate through the Universe. Two-point statistical measures of the observed ellipticities, like the dispersion within a finite aperture or the ellipticity cross-correlation, can be related to the power spectrum of the large-scale structure. The measurement of cosmic shear (especially on small angular scales) can thus be used to constrain cosmological parameters and to test cosmological structure formation in the non-linear regime, without any assumptions about the relation between luminous and dark matter. In this paper we will present preliminary cosmic shear measurements on sub-arcminute scales, obtained from archival STIS parallel data. The high angular resolution of HST, together with the sensitivity and PSF-stability of STIS, allows us to measure cosmic shear along many independent lines-of-sight. Ongoing STIS parallel observations, currently being carried out in the frame of a big GO program (8562+9248), will greatly increase the number of available useful fields and will enable us to measure cosmic shear with higher accuracy on sub-arcminute scales.

1 STIS Parallel Data

Since June 1997, parallel observations using the Space Telescope Imaging Spectrograph (STIS) on the Hubble Space Telescope were taken. The data were non-proprietary and were made available immediately.

The STIS CCD is sensitive to wavelengths ranging from 2500 to 11000 Å and its field of view is $51'' \times 51''$. The STIS CCD pixel size is 50mas.

For the cosmic shear project we selected data sets from June 1997 to 1998 which were taken in the CLEAR filter (unfiltered) and in CR-SPLIT mode. They had to be unbinned, and the associated “jitter ball”, which is a measure of how well the telescope was tracking, was required to have an rms value smaller than 5mas. Images which were taken consecutively during a single telescope visit and which were offset by no more than one quarter of the field of view were grouped into what we refer to as STIS association and coadded using “Drizzle” (see Fruchter & Hook 1998). We obtained 498 coadded associations, which are available at <http://www.stecf.org/projects/shear/>. A detailed description of the data reduction and coaddition procedure can be found in [9].

Starting from these associations, 51 stellar fields and 121 independent galaxy fields were identified. The fields were analysed using both SExtractor [2] and a modified version of the IMCAT package (see [6] (hereafter KSB), [4]). Size and shape parameters were taken from IMCAT, since it was designed specifically to measure robust ellipticities and allows for the correction of measured image ellipticities for shape distortion introduced by the PSF. Positions and magnitudes are estimated with SExtractor. The mean number of selected galaxies per association is 18 on the galaxy fields.

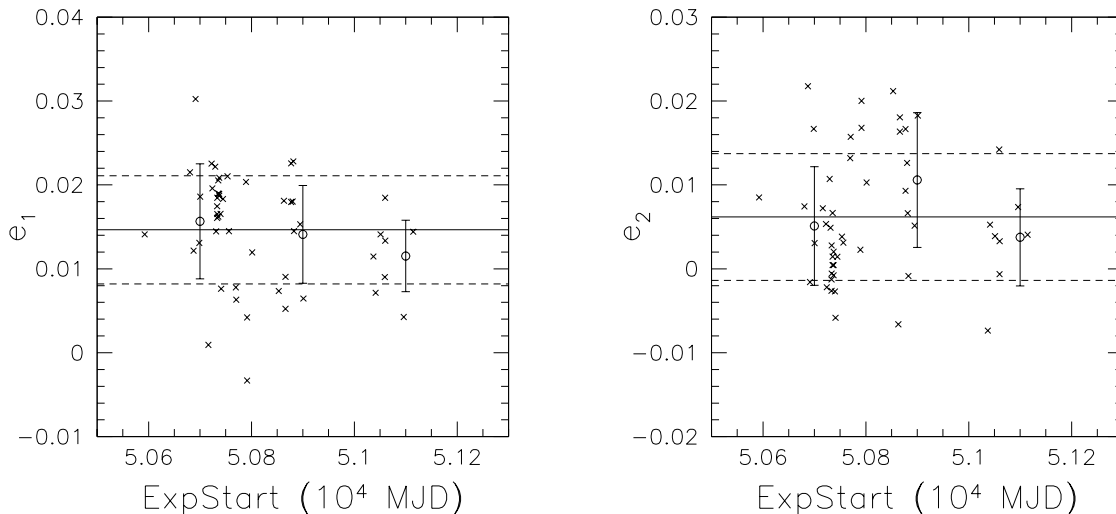


Figure 1: Mean of the ellipticity components e_1 (left) and e_2 (right) of the star fields vs. exposure start time (MJD). The straight lines show the mean over all the fields, the dashed lines show the 1σ dispersion. The circles show the mean over stars in bins between 5.06×10^4 , 5.08×10^4 , 5.10×10^4 , 5.12×10^4 (MJD) with 1σ error bars.

2 PSF correction

The shape of the PSF anisotropy was estimated on the stellar fields using the KSB complex ellipticity parameter e , which is calculated from weighted second order brightness moments.

The total response of a galaxy ellipticity to a shear and the PSF is given by

$$e - e_s = P^\gamma \gamma + P_{sm} q^*, \quad (1)$$

where e and e_s are the observed and intrinsic ellipticities, respectively, and $P^\gamma = P_{sh} - (P_{sh}/P_{sm})^* P_{sm}$, where the shear and the smear polarizability tensors P_{sh} and P_{sm} can be calculated from the galaxy light profile (see KSB). The stellar anisotropy kernel q^* which is needed to correct for PSF anisotropy can be calculated by noting that for stars $e_s^* = 0$ and $\gamma^* = 0$, so that

$$q^* = (P_{sm}^*)^{-1} e^*, \quad (2)$$

In Fig. 1 the mean values over the whole field of the two ellipticity components of stars are shown as a function of the exposure date. The mean ellipticity of all fields is $\approx 1\%$, which is sufficiently small to not significantly affect our cosmic shear analysis. If we divide the star fields into time intervals, the mean ellipticities agree with each other at the 1σ level, therefore the anisotropy can be considered to be constant over the time period covered.

In addition to the variation from field to field (i.e. in time), we also find a spatial variation of the PSF within individual fields. This effect is shown in Fig. 2, middle left panel. We fit the ellipticities with a second-order polynomial at the position $\vec{\theta} = (x, y)$ on the CCD:

$$e_\alpha(\vec{\theta}) = a_{\alpha 0} + a_{\alpha 1}x + a_{\alpha 2}x^2 + a_{\alpha 3}y + a_{\alpha 4}y^2 + a_{\alpha 5}xy, \quad (3)$$

where $\alpha = 1, 2$.

For the individual undrizzled images of some of the star fields we also analysed the PSF anisotropy and find very short timescale variations of the anisotropy pattern over the fields, as can be seen in Fig. 2, bottom panels.

In Fig. 3 we plot the mean ellipticity for all galaxy fields with and without the PSF anisotropy correction. It illustrates that the PSF anisotropy correction changes the mean ellipticity by an amount typically smaller than 1% . Also, the dispersion between different PSF models from different star fields is much less than 1% , which means that the changes of the PSF anisotropy seen in different star fields are sufficiently small to allow us to use one (or a suitable combination of them) for the actual analysis.

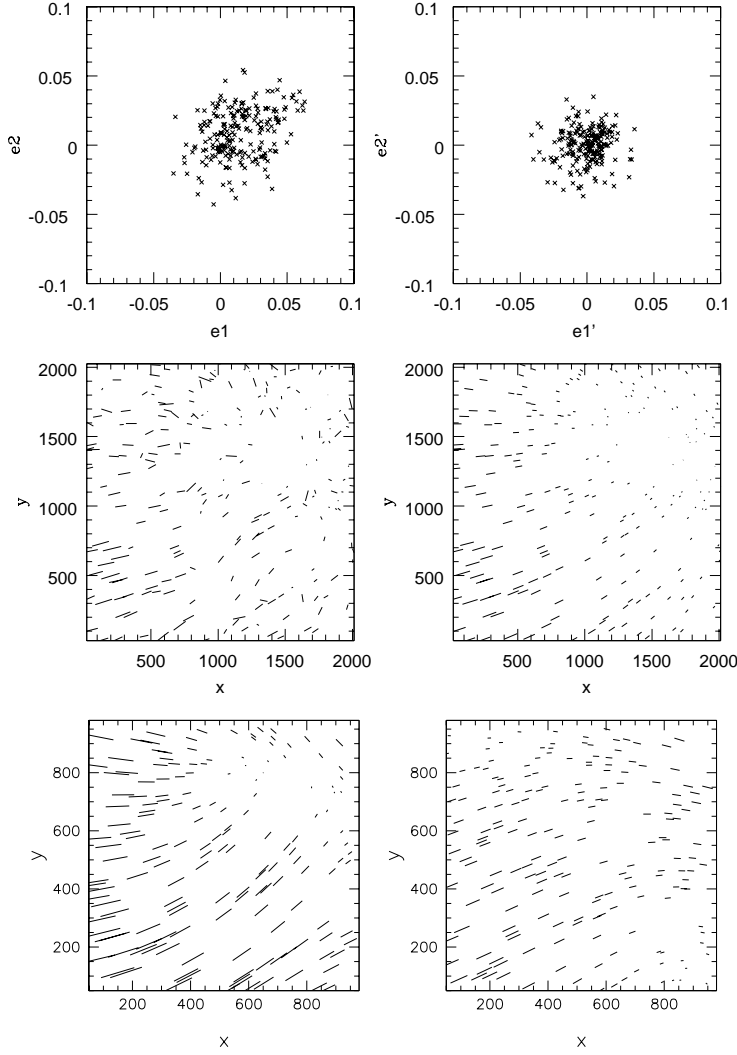


Figure 2: For one star field the distribution of the ellipticities of stars are shown before (top left) and after (top right) correcting for PSF anisotropy. The middle left panel shows the spatial distribution of the ellipticities across the STIS field, the middle right panel the fitted second-order polynomial at the star positions. The length of the sticks indicates the modulus of the ellipticity, the orientation gives the position angle. In the two plots at the bottom we show the values of the polynomials for the anisotropy correction of two individual, undrizzled exposures of the star field. The two individual fields were taken with a time difference of only 30 minutes and demonstrate the very short timescale variations of the PSF anisotropy pattern.

The smearing corrected ellipticity of each galaxy is calculated by

$$e^{\text{iso}} = (P^\gamma)^{-1}(e - P_{\text{sm}}q^*), \quad (4)$$

which is an unbiased (provided that $\langle e_s \rangle = 0$) but very noisy estimate of the shear γ .

To check that we did not introduce systematics in our galaxy selection and PSF correction we also calculated the probability distribution for all galaxy ellipticities which were used in the cosmic shear analysis and found that the mean ellipticity is compatible with zero, and the dispersion in both components is $\sigma_1 = \sigma_2 = 26\%$.

3 Cosmic Shear

The rms shear in a circular aperture with angular radius θ is related to the power spectrum of the surface mass density κ by

$$\langle \bar{\gamma}^2 \rangle (\theta) = 2\pi \int_0^\infty ds s P_\kappa(s) [I(s\theta)]^2, \quad (5)$$

where $I(\eta) := J_1(\eta)/(\pi\eta)$ and J_1 is the Bessel function of the first kind. P_κ in turn is related to the three-dimensional power spectrum by a simple projection:

$$P_\kappa(s) = \int_0^{w_H} dw g(w) P\left(\frac{s}{f_K(w)}; w\right), \quad (6)$$

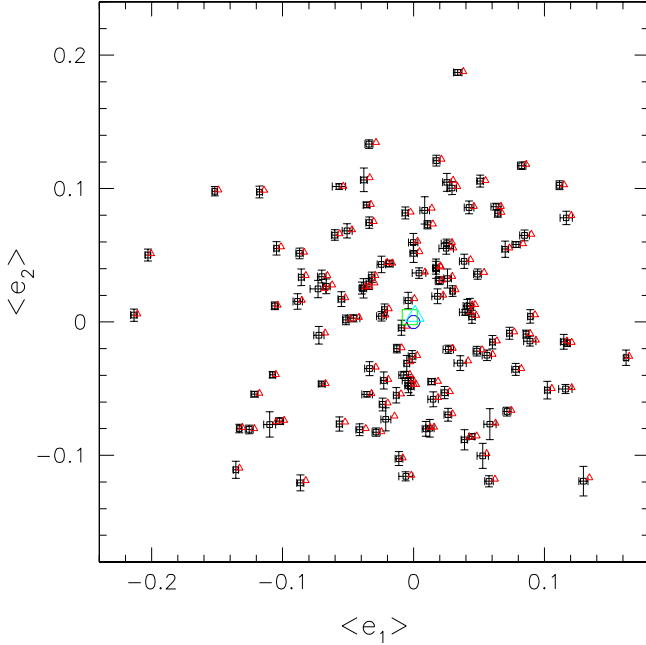


Figure 3: For the galaxy fields we plot the mean uncorrected ellipticity of galaxies (triangles) as well as the mean anisotropy corrected ellipticity (squares). The error bars attached to the squares denote 3 times the dispersion of the field-averaged corrected ellipticities when the different PSF model fits are used. The error on the mean is much smaller than the symbols used. The shift of the corrected mean ellipticities toward negative e_1 is expected from the behaviour of the stellar ellipticities plotted in Fig. 1. The big triangle and big square in the centre denote the mean over all galaxy fields of the uncorrected and corrected mean ellipticities, respectively; the size of the symbols represent the 1σ errors on the mean. The circle shows the origin for reference.

where w is the comoving distance, $f_K(w)$ is the comoving angular diameter distance, $g(w)$ includes geometrical factors which depend on the redshift distribution of the sources (see [10]), and the integral extends to the horizon w_H .

Let e_{in} denote the fully corrected ellipticity of the i -th galaxy on the n -th field, then the quantity we measure for each field is

$$\bar{\gamma}_n^2 := \frac{\sum_{i \neq j} w_{in} w_{jn} e_{in} e_{jn}^*}{\sum_{i \neq j} w_{in} w_{jn}}, \quad (7)$$

where w_{in} is the weight of the i -th galaxy in the n -th field. This is an unbiased estimate of the cosmic shear dispersion in the n -th field. Note that $\bar{\gamma}_n^2$ is not positive definite. From this one obtains an unbiased estimate of the cosmic shear dispersion:

$$\langle \bar{\gamma}^2 \rangle = \frac{\sum N_n \bar{\gamma}_n^2}{\sum N_n}, \quad (8)$$

where we weight each galaxy field by the number of galaxies per field N_n to minimize Poisson noise.

Using all 121 galaxy fields we find an rms cosmic shear of $\sim 4\%$ with 1.5σ significance. Restricting the analysis to fields with higher number density of galaxies we find a larger cosmic shear signal. This would agree with a cosmological interpretation of the signal: Fields with a higher number density of objects typically have a larger exposure time, therefore they typically probe higher redshifts and one expects a higher cosmic shear signal.

If we apply the PSF corrections from different star fields individually we find that the difference between the star field corrections is much smaller than the statistical error on the cosmic shear measurement, which again demonstrates that PSF effects of STIS are small.

In Fig. 4 we compare our result for the cosmic shear to the ones obtained by other groups on larger scales and to the theoretically expected values when using different cosmological models with a mean source redshift of $\langle z_s \rangle = 1.2$, which is appropriate for the ground-based measurements. With the STIS data we are probably probing at higher mean redshifts, but since our observations with STIS were taken in the CLEAR filter mode, we do not have any information about the exact redshift range of our galaxies. Moreover, our fields have a large spread in exposure times and therefore we effectively average over different cosmic shear values. The galaxies on fields with longer exposure times are expected to probe higher redshifts on average. Their light bundles traverse a larger amount of matter, and therefore we expect a higher value for the cosmic shear. Multicolour observations from the ground have been carried out to determine the redshift distribution of galaxies in the STIS fields photometrically. With these, we will be able to quantitatively interpret the cosmic shear measurement relative to other angular scales.

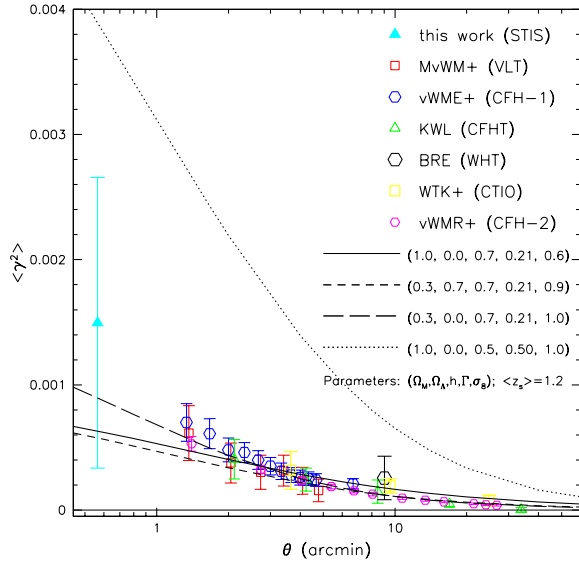


Figure 4: Comparison of our cosmic shear result with measurements at larger angular scales from other groups and with model predictions. The lines show the theoretical predictions if one uses different cosmological models, which are characterized by Ω_m , Ω_Λ , h , Γ and σ_8 . The redshift distribution is taken from [3], with a mean source redshift of $\langle z_s \rangle = 1.2$.

Although we obtained a detection of the cosmic shear, the error bar is still large. The error in the data depends both on the number of galaxies per field and on the number of fields. It is therefore important to get more fields with higher number densities of objects. The parallel observations with STIS are currently continued with a GO cycle 9 parallel proposal (8562+9248, PI: P. Schneider).

Acknowledgements. We thank Y. Mellier and L. van Waerbeke for fruitful discussions. This work was supported by the TMR Network ‘‘Gravitational Lensing: New Constraints on Cosmology and the Distribution of Dark Matter’’ of the EC under contract No. ERBFMRX-CT97-0172 and by the German Ministry for Science and Education (BMBF) through the DLR under the project 50 OR106.

References

- [1] Bacon, D., Refregier, A., Ellis, R.S., 2000, MNRAS, 318, 625 (BRE)
- [2] Bertin, E., Arnouts, S., 1996, A&AS, 117, 393
- [3] Brainerd, T.G., Blandford, R.D., Smail, I., 1996, ApJ, 466, 623
- [4] Erben, T., van Waerbeke, L., Bertin, E., Mellier, Y., Schneider, P., 2001, A&A, 366, 717
- [5] Fruchter, A.S., Hook, R.N., submitted to PASP, astro-ph/9808087
- [6] Kaiser, N., Squires, G., Broadhurst, T., 1995, ApJ, 449, L105
- [7] Kaiser, N., Wilson, G., Luppino, G.A., 2000, submitted to ApJ, astro-ph/0003338
- [8] Maoli, R., van Waerbeke, L., Mellier, Y., Schneider, P., Jain, B., Bernardeau, F., Erben, T., Fort, B., 2001, A&A, 368, 766 (MvWM)
- [9] Pirzkal, N., Collodel, L., Erben, T., Fosbury, R.A.E., Freudling, W., Hämmerle, H., Jain, B., Micol, A., Miralles, J.-M., Schneider, P., Seitz, S., White, S.D.M., 2001, A&A, 375, 351 (Paper I)
- [10] Schneider, P., van Waerbeke, L., Jain, B., Kruse, G., 1998, MNRAS, 296, 873
- [11] van Waerbeke, L., Mellier, Y., Erben, T., Cuillandre, J.C., Bernardeau, F., Maoli, R., Bertin, E., Mc Cracken, H.J., Le Fèvre, O., Fort, B., Dantel-Fort, M., Jain, B., Schneider, P., 2000, A&A, 358, 30 (vWME)
- [12] van Waerbeke, L., Mellier, Y., Radovich, M., Bertin, E., Dantel-Fort, M., Mc Cracken, H.J., Le Fèvre, O., Foucaud, S., Cuillandre, J.C., Erben, T., Jain, B., Schneider, P., Bernardeau, F., Fort, B., 2001, A&A, 374, 75 (vWMR)
- [13] Wittman, D.M., Tyson, J.A., Kirkman, D., Dell’Antonio, I., Bernstein, G., 2000, Nature, 405, 143 (WTK)